

## Numerical simulation of hollow steel profiles for lightweight concrete sandwich panels

E. Brunesi<sup>\*1</sup>, R. Nascimbene<sup>2a</sup>, M. Deyanova<sup>1b</sup>,  
C. Pagani<sup>3c</sup> and S. Zambelli<sup>3d</sup>

<sup>1</sup>ROSE Programme, UME School, IUSS Pavia, Institute for Advanced Study Via Ferrata 1,  
27100 Pavia (PV), Italy

<sup>2</sup>EUCENTRE, European Centre for Training and Research in Earthquake Engineering Via Ferrata 1,  
27100 Pavia (PV), Italy

<sup>3</sup>B.S.Italia, Styl-Comp group Via Stezzano 16, 24050 Zanica (BG), Italy

(Received October 21, 2014, Revised February 3, 2015, Accepted April 20, 2015)

**Abstract.** The focus of the present study is to investigate both local and global behaviour of a precast concrete sandwich panel. The selected prototype consists of two reinforced concrete layers coupled by a system of cold-drawn steel profiles and one intermediate layer of insulating material. High-definition nonlinear finite element (FE) models, based on 3D brick and 2D interface elements, are used to assess the capacity of this technology under shear, tension and compression. Geometrical nonlinearities are accounted via large displacement-large strain formulation, whilst material nonlinearities are included, in the series of simulations, by means of Von Mises yielding criterion for steel elements and a classical total strain crack model for concrete; a bond-slip constitutive law is additionally adopted to reproduce steel profile-concrete layer interaction. First, constitutive models are calibrated on the basis of preliminary pull and pull-out tests for steel and concrete, respectively. Geometrically and materially nonlinear FE simulations are performed, in compliance with experimental tests, to validate the proposed modeling approach and characterize shear, compressive and tensile response of this system, in terms of global capacity curves and local stress/strain distributions. Based on these experimental and numerical data, the structural performance is then quantified under various loading conditions, aimed to reproduce the behaviour of this solution during production, transport, construction and service conditions.

**Keywords:** precast panel; composite panel; steel profile; shear response; void shape; FE models; interface elements

### 1. Introduction

Precast concrete panels have been used since decades as a common cladding solution to enclose the exterior façade of structural systems, being the desired architectural expression provided, in a

---

\* Corresponding author, Ph.D. Student, Email: [emanuele.brunesi@eucentre.it](mailto:emanuele.brunesi@eucentre.it)

<sup>a</sup> Ph.D., Email: [roberto.nascimbene@eucentre.it](mailto:roberto.nascimbene@eucentre.it)

<sup>b</sup> Ph.D. Student, Email: [manya.deyanova@umeschool.it](mailto:manya.deyanova@umeschool.it)

<sup>c</sup> MEng, Email: [ufftecnico06@styl-comp.it](mailto:ufftecnico06@styl-comp.it)

<sup>d</sup> MEng, Email: [ufftecnico06@styl-comp.it](mailto:ufftecnico06@styl-comp.it)

practical and economical way, by special shapes and uniform finishes (PCI, 2007). This applies even to a greater extent to the case of multi-layered or so-called sandwich panels, which consist of thermal and/or noise insulating layers protected from external environmental conditions by a series of external and internal reinforced concrete (RC) layers. Usually, they fall in the category of non-structural components and, in the past, the design of such systems was only based on concepts of “good-design-practice”, out of specific prescriptions in Codes and/or Standards. As a consequence, major seismic events, in the Italian territory, have shown their poor performance (Liberatore *et al.* 2013, Magliulo *et al.* 2014, Bournas *et al.* 2014, Belleri *et al.* 2014), reaffirming seismic vulnerabilities emerged in other destructive earthquakes (Adalier and Aydingun 2001, Sezen and Whittaker 2006, Ghosh and Cleland 2012, Toniolo and Colombo 2012). Under operational conditions, these panels resist self-weight and out-of-plane wind-induced forces to be transferred to the supporting structure. Without the ability to accommodate relative displacement, panels attract unintended forces, causing them to fail and fall from the structure (Brunesi *et al.* 2015a), particularly when associated with high out-of-plane slenderness, as no lateral restraint was provided in correspondence to columns and RC spandrels, in old buildings.

The severe damage suffered as a consequence of inadequate stiffness, strength and ductility of these systems and/or insufficient connections detailing implies the need for specific procedures to assess their capacity and mitigate intrinsic structural deficiencies. In the last two decades, a better understanding of the importance of the façade panels in the global structural behaviour and design has been developed (Henry and Roll 1986, Charney and Harris 1989, Taghavi and Miranda 2003, Hunt and Stojadinovic 2010, Brunesi *et al.* 2015a). Non-structural components have more recently attracted significant research efforts to characterize their response under seismic loads, experimentally (Mosqueda *et al.* 2009, Retamales *et al.* 2011, 2013, Petrone *et al.* 2014) and numerically (Villaverde 2006, Medina *et al.* 2006, Wanitkorkul and Filiatrault 2008), thus showing them to play a relevant and active role in the response and, therefore, design of the entire building, in terms of both structural periods and lateral displacements.

Different building typologies and configurations may be differently affected by different façade systems and technologies, according to stiffness and strength of panel-to-structure connections and cladding solution itself which, for composite systems such as sandwich panels, may be not so easy to estimate, even if they represent crucial parameters for their design or the assessment of existing systems, for what concerns damage pattern and related repairing costs. In light of this scenario, the aim of this study is to characterize both global and local behaviour of a precast composite concrete sandwich panel, from an Italian supplier, under shear, tensile and compressive loads, by a series of detailed 3D brick FE models, based on nonlinear fracture mechanics. Geometrically and materially nonlinear analyses have been performed on both prototypes, representative of this technology, and their subassemblies. Nonlinear constitutive laws have been calibrated on preliminary experimental characterization tests of panel components and, then, numerical simulations have been carried out, on whole specimens, in compliance with experimental observations used to validate the modeling approach proposed. Finally, structural performance is assessed during manufacturing and erection stages, as well as service conditions, which still remain crucial aspects for their design, in areas of moderate seismicity.

## 2. Behaviour in shear

The panel investigated consists of external and internal RC layers, coupled by a series of

cold-drawn steel profiles with an intermediate thermal insulating layer of polystyrene, as shown in Fig. 1, where a schematic of this composite technology, with its key components, is provided. Hence, a specimen, whose geometrical characteristics are summarized in the following, is constructed using this solution, and then tested in shear to evaluate the ability of the transverse C-shaped steel profile to couple the two RC layers. The stress-strain constitutive laws implemented for steel and concrete are based on well-known models calibrated in accordance with the results of pull and pull-out tests performed on steel ties and steel ties-concrete blocks, presenting material properties representative of those used for the prototypes tested experimentally. Details concerning test setup and procedure, as well as a brief description of specimens, materials and reinforcement layout, will be given in the following.

### 2.1 Experimental investigation of panel subassemblies

Shear tests were conducted on a small portion of the panel under investigation. In particular, the reference specimen consisted of a 600x1000 mm panel subassembly, characterized by 80 mm thick internal and external concrete layers, reinforced by means of a 150x150 mm grid composed of  $\varnothing 5$  bars. To couple these two RC blocks, two 500 mm long steel profiles were embedded into them, as presented in Fig. 2. The mean 28-day concrete compressive strength ( $f_c$ ) was measured to be equal to 35 MPa, whilst the steel profile, cold-formed from a stainless steel sheet named in the upcoming discussion as “ECO210 INOX”, showed mean tensile strength of 326 and 510 MPa, at 0.2% strain ( $f_{0.2\%}$ ) and at ultimate conditions ( $f_u$ ), respectively. Traditional B450C mild steel was used for mesh reinforcement. Insulating polystyrene layers were conservatively assumed to add any contribution, in terms of bearing capacity, and, hence, omitted in the specimens tested.

The reference prototype was subjected to in-plane shear deformation restraining the internal RC layer, at top and bottom, whilst two actuators were used to apply a monotonically increased tensile force at the top of the external concrete block. A set of stiff beams was provided along the edges of the fixed side to prevent any undesirable local mechanism, additionally permitting a more uniform transfer of the load path. The experimental test setup is schematized in Fig. 2.

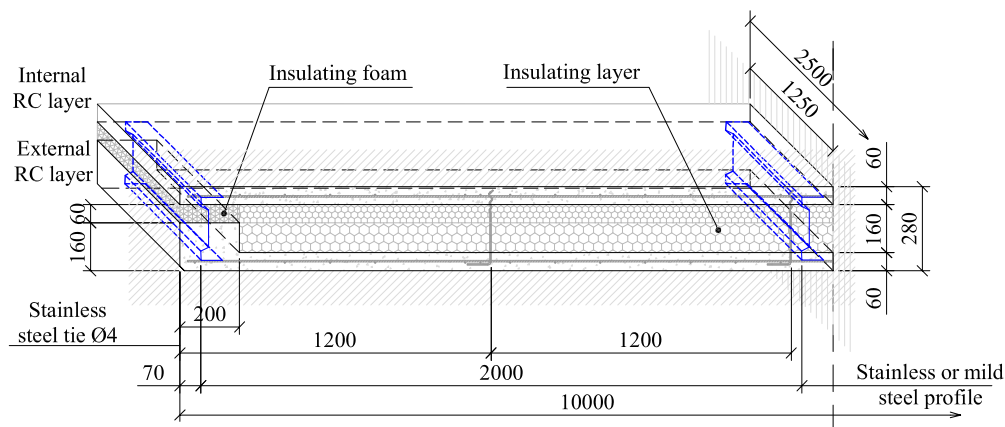


Fig. 1 Schematic of the sandwich panel analyzed

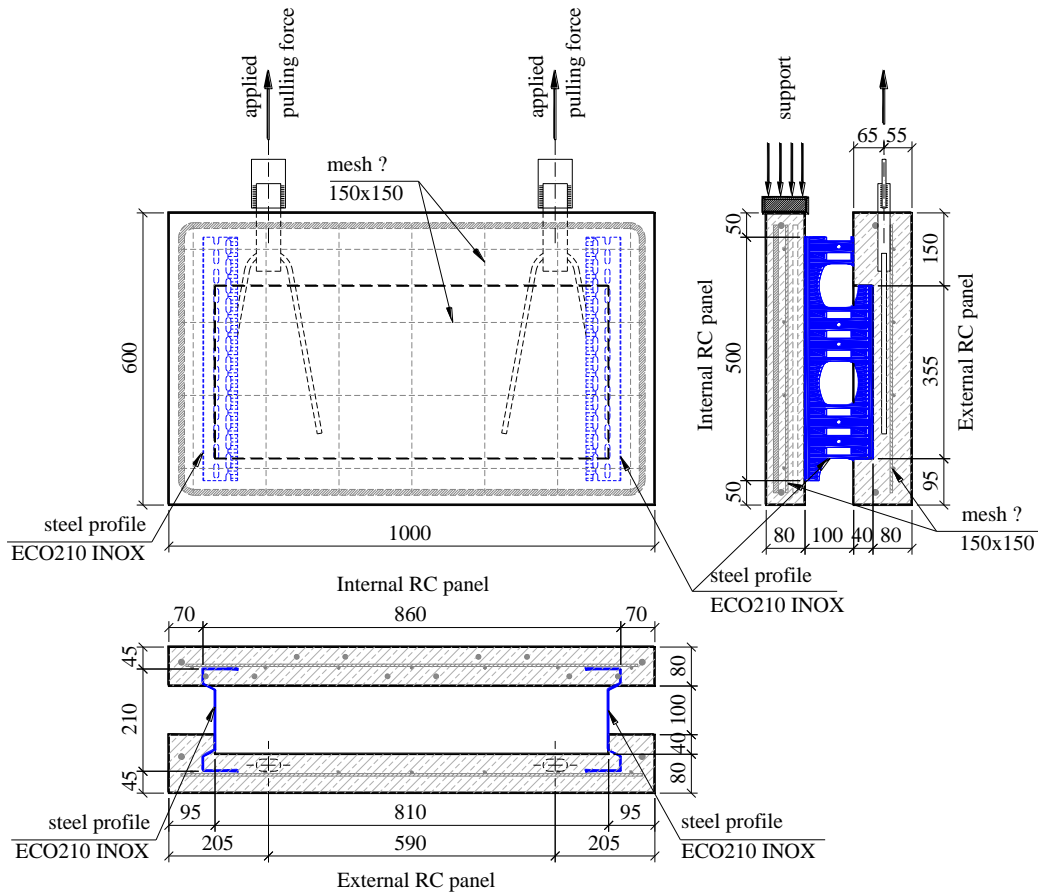


Fig. 2 Schematic of the specimen and experimental test setup

## 2.2 Nonlinear monotonic solid FE analyses

The experimental loading protocol, applied in displacement control, was reproduced by a series of detailed 3D numerical models developed within a well-established general purpose FE package MIDAS FEA (MIDAS 2010). Six-node brick elements were used to mesh concrete layers and steel profiles, whilst one-dimensional embedded elements and two-dimensional interface elements were assumed to represent mesh reinforcement and steel profile-concrete layers interaction, respectively.

Nonlinear fracture mechanics was proven to be a transparent and effective manner for modeling the inelastic behaviour of concrete in several applications (Hung and El-Tawil 2010, Hung and Li 2013, Hung *et al.* 2013, Biscaia *et al.* 2013, Le Nguyen *et al.* 2014, Pecce *et al.* 2014, Brunesi *et al.* 2015b, 2014a). In this work, the total strain crack (TSC) model, implemented along the lines of the modified compression field theory (Vecchio and Collins 1986), was adopted taking advantage of a diffuse smeared fixed cracking approach able to simultaneously account for both normal and shear stresses on potential crack surfaces. The models proposed by Thorenfeldt *et al.* (1987) and Hordijk (1991) were used for uniaxial compressive and tensile behaviour, respectively. Figs. 3 and 4

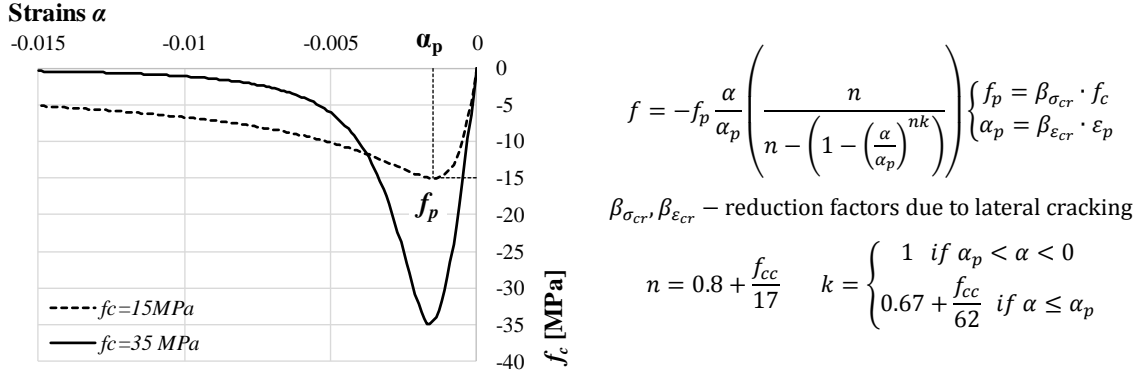


Fig. 3 Compressive stress-strain relationships for TSC model

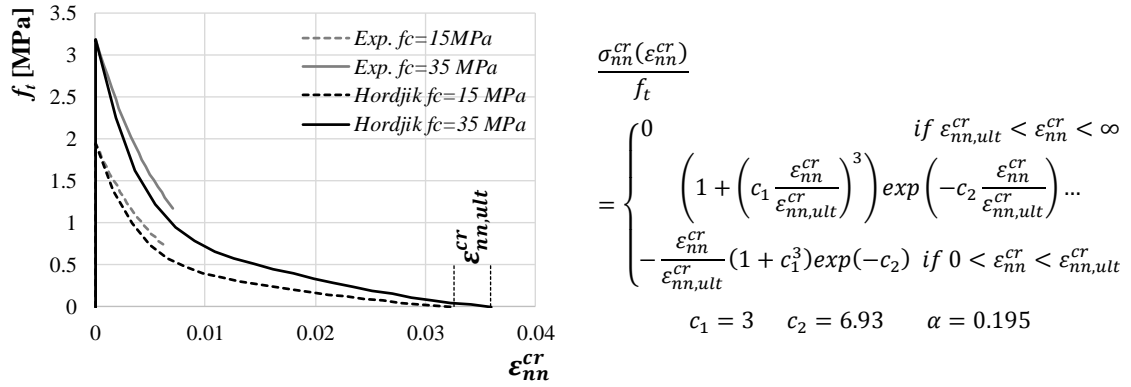


Fig. 4 Tensile stress-strain relationships for TSC model

present their calibration, in accordance with CEB-FIP Model Code (1990). Two compressive strengths (i.e. 15 and 35 MPa) were assumed as representative of concretes with different aging used for pull-out and shear tests. In addition, a comparison is provided between an exponential softening curve and Hordijk model, showing the latter to lead to slightly more conservative values of tensile strength ( $f_t$ ) for the same crack strain. Both confinement and lateral crack effect were accounted in the series of numerical simulations, according to Vecchio and Collins (1993).

A classical Von Mises yielding criterion, combined with isotropic strain hardening (Venini and Nascimbene 2003), was adopted to include material nonlinearities of both steel profiles and mesh reinforcement. The assumed true stress-strain constitutive laws (Girão Coelho 2013, Brunesi *et al.* 2014b, 2015c) were calibrated on properties from the characterization tests performed by the producer, for both stainless and mild steel.

Two-dimensional zero-thickness interface elements were introduced to represent concrete-steel interaction, through a bond-slip constitutive model able to reproduce, in a phenomenological sense, formation and evolution of transverse and longitudinal cracks in the vicinity of the embedded steel material. Based on total deformation theory, this approach expresses tractions as a function of total relative displacements. In particular, the relationship between normal traction and normal relative displacement is assumed to be linear elastic in compression only, whereas the relationship between shear traction and slip is imposed to be a cubic polynomial function, according to Dörr (1980) (see

Fig. 5).

An energy-normalized convergence criterion, with a threshold set equal to  $10^{-3}$ , was adopted to equilibrate loads through an incremental iterative procedure; Newton-Raphson algorithm was used to perform the implicit solution strategy. Hence, even if classical fiber-based models (Spacone *et al.* 1996) are effective and time-saving solutions to assess the global response of different types of RC structures (Casarotti and Pinho 2006, Mpampatsikos *et al.* 2008, Brunesi and Nascimbene 2014), a high-definition FE model is an attractive tool for investigation of collapse mechanisms, being able to predict stress-strain distributions and the related evolution of damage patterns. In the following, these local quantities, crucial in interpreting failure modes, will be examined and discussed, after a preliminary validation of the numerical approach proposed.

### 2.2.1 Calibration of FE models

To validate the calibration of the constitutive laws assumed, two preliminary experimental tests on panel components were numerically reproduced. First, static pull tests were performed on a  $\varnothing 4$ , 250 mm long, stainless steel AISI 302 tie. In Table 1, its geometry is shown, as well as a schematic of the experimental test setup. A mesh of six-node tetrahedrons was swept to materialize its double S-shaped end, and perfect boundary conditions were introduced to restrain its gripped parts both at top and bottom, thus allowing only 210 mm of its length to axially deform between the jaws of the testing apparatus. A detail of FE mesh and boundary conditions is provided in Table 1, as well as a comparison between experimental and numerical capacity, at ultimate conditions. Similarly, Fig. 6 compares FE and experimental observations in terms of tensile load-axial displacement curves and

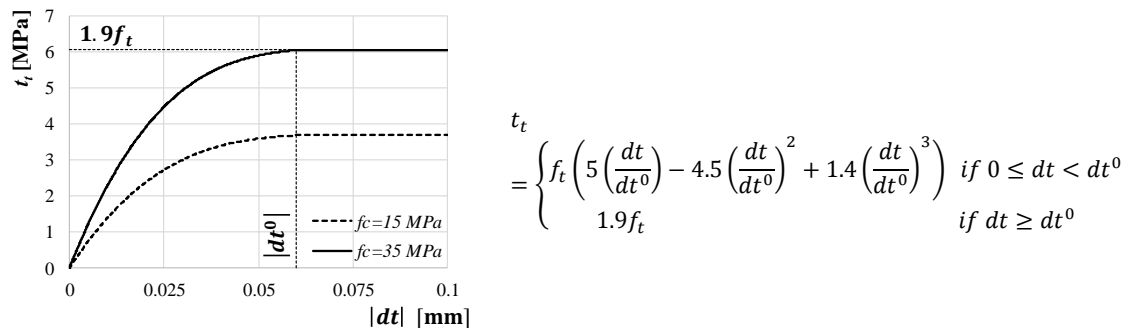


Fig. 5 Bond-slip constitutive law for interface elements

Table 1 Ultimate tensile capacity of the stainless steel tie from tests and numerical model

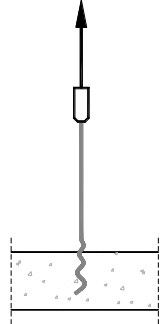
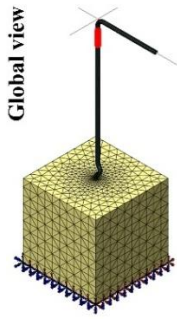
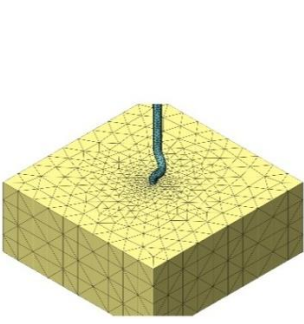


Tie	Experimental Test	Numerical model	
		#	$F_{ultimate}$ [kN]
		1	17.6
		2	17.8
		3	17.9
			$F_{ultimate}$ [kN]
			17.5

failure mechanism. At moderate displacements, slip occurs until the ties go into bearing in the jaws, with a visible load picking up in the experimental capacity curves. By contrast, numerical curve is stiffer at these stages, being the load transfer immediately induced by perfect boundary conditions. As the applied axial displacement monotonically increases, the S-shaped portion of the tie deforms and opens up, thus showing large strain concentrations. This mechanism is slightly more gradual in the numerical analysis, characterized by a quite smooth curve up to failure, while the experimental curves more suddenly drop, when large strains take place in correspondence to this disturbed zone. A close correlation with FE results is obtained, particularly if the experimental curve with the least initial slip is considered, since almost identical trends are observed. In addition, a mismatch within 2% is shown, in terms of ultimate tensile strength. Both large displacement-large strain kinematics and Von Mises yielding criterion with isotropic strain hardening appear effective and conservative, when applied to predict the experimental response of this component, controlled by a combination of material and geometric nonlinearities. A satisfying agreement is predicted between experimental bottleneck damage patterns and principal tensile and compressive strain distributions, as evidenced in Fig. 6, whose legend denotes the portions of volume (i.e. % Vol.) experiencing the strain ranges specified.

Then, a series of pull-out tests, conducted on the stainless steel tie previously studied in tension, were considered and their results were used to quantify the effectiveness of the constitutive models assumed for concrete and steel-concrete interaction. The curved part of the steel tie was embedded in a concrete block, whose compressive strength was measured to be 15 MPa, and a monotonically increased pulling force was applied on the other side of the dowel until visible cracks occurred and resulted into a partial expulsion of the concrete. Table 2 schematically presents pull-out test and its numerical representation. The concrete cube (i.e. 1x1x1 m) was chosen to be much greater than the volume disturbed during the experimental test. Calibration of compressive and tensile behaviour of concrete can be observed in Fig. 3 and 4, respectively. Fig. 5 shows the relationship between shear traction and slip implemented for the interface elements.

As evidenced in Fig. 7, a maximum tensile resistance of about 10 kN is determined numerically, while experimental predictions approximately vary between 8 and 10 kN. FE estimate highlights a satisfying and safe fit with test observations, being the tensile load-axial displacement curve much closer to the conservative branch of the experimental fork. Principal tensile and compressive strain distributions predicted at ultimate conditions are collected in Fig. 8.

Table 2 Pull-out test and FE idealization

Pull-out Test		Numerical model		
				

Pronounced concentrations are obtained in the concrete adjacent to the double S-shaped part of the stainless steel tie. Furthermore, the evolution of the crack pattern at increasing displacement steps is shown in Fig. 9. Initial cracks appear at roughly 2 kN and propagate radially, thus resulting into a cracked concrete cone (see Fig. 10, left); as the tensile force applied increases, its radius increases (Fig. 10, center), while the stress experienced decreases, being the concrete more severely damaged. At ultimate conditions (Fig. 10, right), major cracks developed and the tie begins to slip, because the surrounding concrete loses its capability for shear force transfer (i.e. cracks in blue).

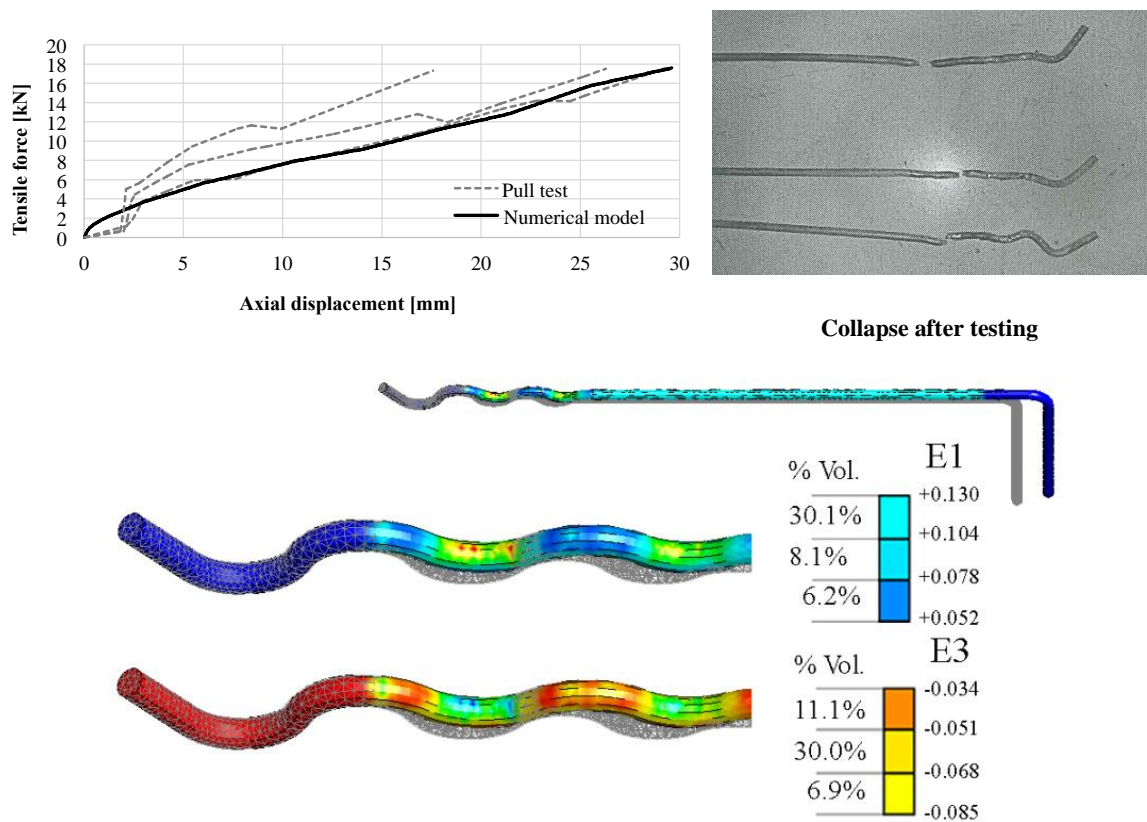


Fig. 6 Stainless steel tie AISI 302: capacity curves and collapse mechanism

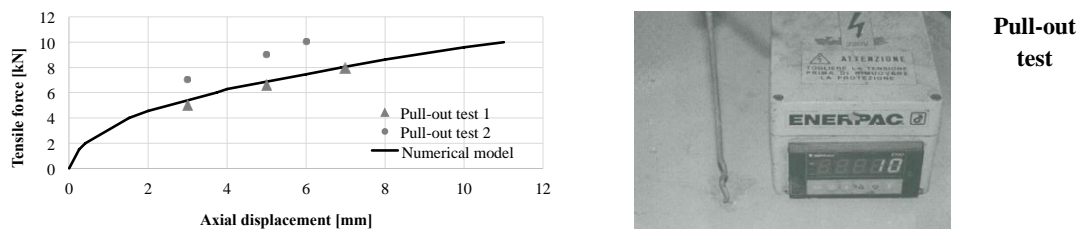


Fig. 7 Pull-out test: capacity curves



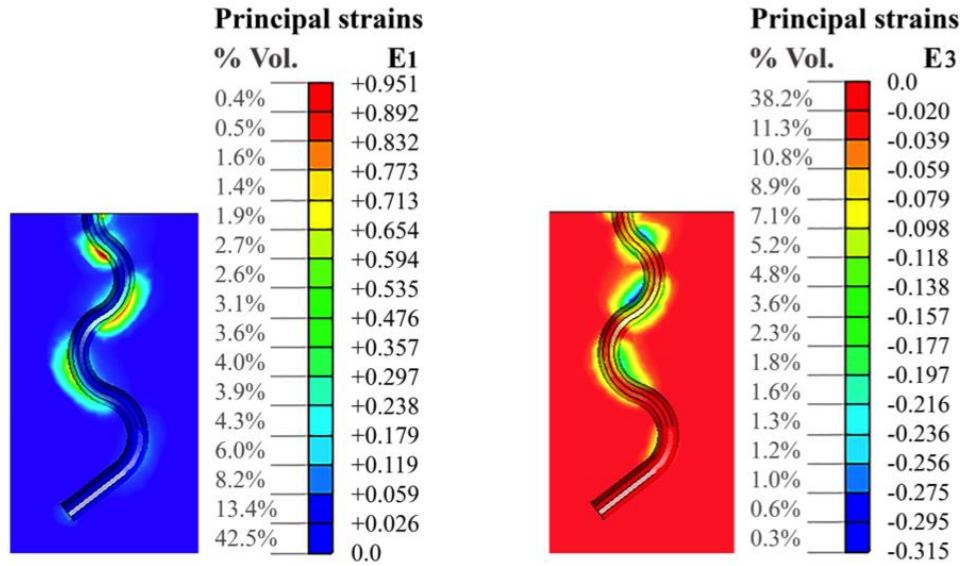


Fig. 8 Principal tensile (left) and compressive (right) strains in concrete, at ultimate conditions

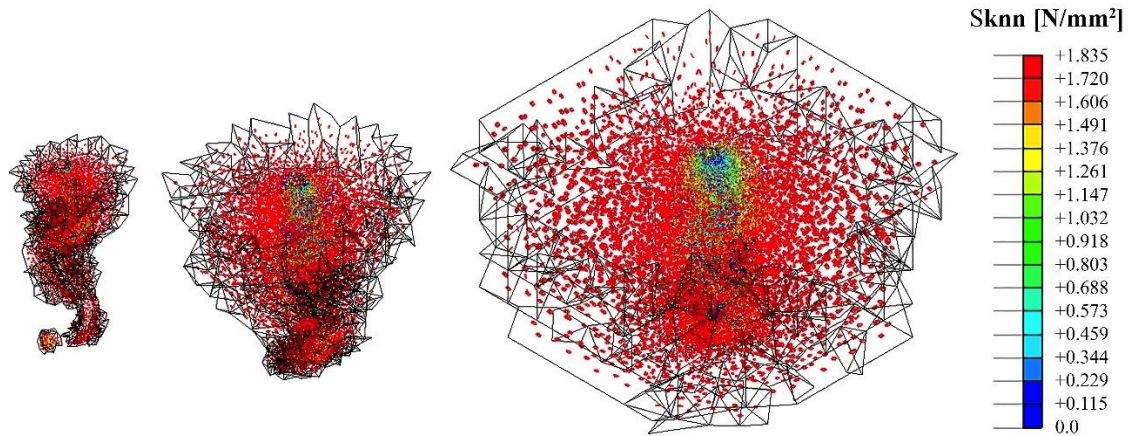


Fig. 9 Development of crack patterns in the concrete block

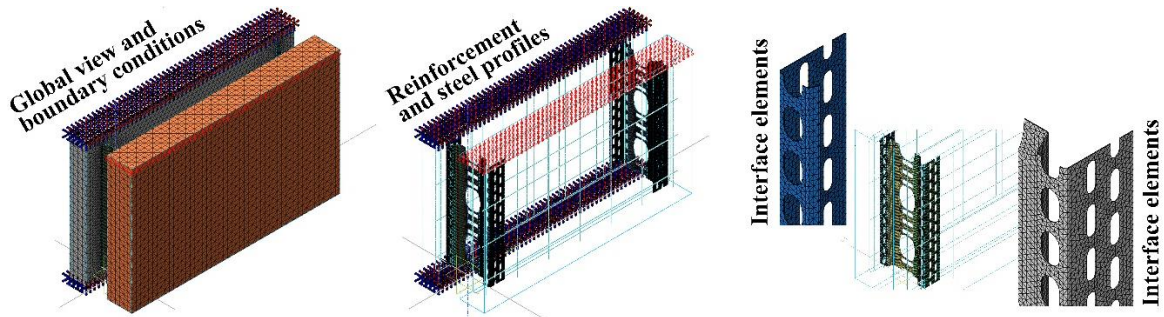


Fig. 10 Example of FE model: global view and details – Specimen 600x1000 mm

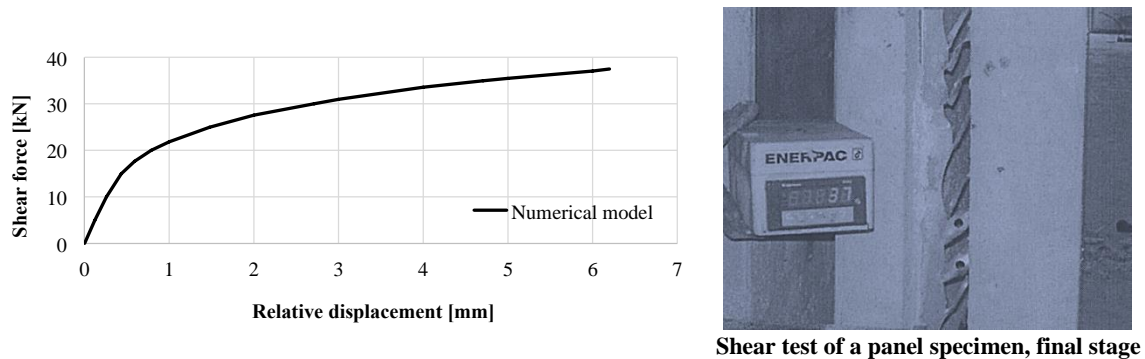


Fig. 11 Shear force-displacement capacity curve – Specimen 600x1000 mm

### 2.2.2 Shear response: results and discussion

Numerical techniques and constitutive laws previously detailed and validated were employed to predict the experimental response of the 600x1000 mm panel subassembly described in Paragraph 2.1. An example of the high-definition FE model prepared, with its basic components, is presented in Fig. 10. Details of the mesh used for concrete layers, steel profiles, interface elements and mesh reinforcement are shown herein; their stress-strain relationships were calibrated in accordance with material properties specified in Section 2.1 (Figs. 3-5). A uniformly distributed displacement was applied on top of the external concrete layer to perform the simulation, in large displacement-large strain mode.

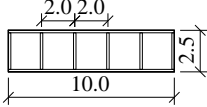
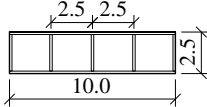
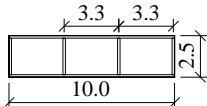
Fig. 11 compares the experimental and numerical shear capacities obtained for the prototype. In detail, the ultimate resistance equals 37.0 kN and 37.5 kN, respectively, thus revealing an accurate agreement between test and FE estimates. The modeling approach proposed appears to be effective for shear strength assessment of this composite solution, as additionally proven by the comparison between numerically predicted and experimentally observed collapse mode. In Fig. 12, Von Mises stress and principal tensile strain distributions closely match the experimental damage pattern. The following criteria were assumed as conservative checks of the “near collapse” limit state

- 1) First exceedance of a conventionally fixed ultimate strain limit in concrete and steel.
- 2) Excessive in-plane and out-of-plane distortion of the profiles.
- 3) Excessive slippage between stainless steel profiles and concrete layers.

Values of  $5 \cdot 10^{-3}$  and  $8 \cdot 10^{-2}$  were conservatively selected as the ultimate concrete and steel strain, respectively. Being the layer-to-layer distance set as 100 mm, displacements of up to 6 mm and 0.1 mm were used to compute the maximum global in-plane and out-of-plane distortion of the profiles, respectively. A shear slip of about 0.1 mm was chosen to be the conventional ultimate steel profile-concrete layer slippage. Therefore, failure of the system was assumed to occur when the first of the three conditions happened.

In this simulation, the first two criteria (i.e. exceedance of the conventional ultimate steel strain and in-plane deformation of the profiles) were observed to roughly coincide, since global and local conditions almost simultaneously took place, thus implying a quite balanced failure mechanism. In particular, the high plastic strain concentrations obtained in the hole-pattern of the steel profiles, as a consequence of the strut-and-tie path developed, did not cause any anticipated net fracture in the

Table 3 Shear capacity vs. demand on a steel profile as part of the panel

Analysis type	Steel grade	$F_{s,y}$ [kN/m]	$M_s$ [kNm/m]	$F_s$ due to self-weight of the external RC layer [kN/m]
Strip S1	Mild steel S250GD+Z	23	13.8	
Strip S2	$f_{0,2\%} = 271$ MPa	48	2.9	
Subassembly 600x1000 mm	Stainless steel ECO210 INOX $f_{0,2\%} = 326$ MPa	22	3.1	

profile itself, which was conversely shown to exhibit a gradual evolution of its deformation pattern. Moderate out-of-plane distortions were predicted both experimentally and numerically until global collapse was undergone. Concrete experienced no damage except minor cracking in small volumes adjacent to the profiles, where stress levels slightly less than peak tensile strength were still able to be transmitted across the cracks and, in addition, reinforcing mesh was found to behave elastically, at negligible stress rates of approximately 9 MPa.

To further confirm this behaviour, the shear response of a single profile was analyzed, assuming boundary and loading conditions representative of those applied to the subassembly. Geometry and material properties remained unchanged, while the portion embedded into the internal and external concrete layers were restrained and loaded, respectively. A uniform displacement pattern was used to test the stainless steel profile in shear, thus verifying the role played by the steel profile-concrete blocks slippage to be almost negligible for this composite technology. As observed in Fig. 13, Von Mises stress distributions in close agreement with those collected in Fig. 12 were obtained in terms of path and intensity. Almost identical trends are shown by the shear force-displacement curves for global and simplified FE models, presenting a mismatch within 1%, for what concerns the ultimate shear capacity (i.e. 37.5 kN vs. 37.9 kN). As a result, perfect bond between the two components of this system took place within the entire displacement range.

Sensitivity of shear response to material characteristics and concrete layer-to-layer distance was then quantified by considering two representative stripes, namely “S1” and “S2”, extracted from a 10x2.5 m panel, whose six profiles, spaced of 2 m, were composed of mild steel ( $f_{0,2\%} = 271$  MPa). A schematic of the panel selected and details of the high-definition FE mesh prepared are provided in Fig. 14. Geometry and hole-pattern of the profiles were kept constant, while their embedment is different, being the two segments placed at inner and outer positions, respectively. In detail, block-to-block clearance was equal to 160 and 60 mm for S1 and S2, respectively. Boundary and loading conditions were imposed at the lateral sides of the 2.5 m long stripes considered in order to inhibit any secondary mechanism and, hence, determine the potential for shear force transfer of

these two mild steel profiles, when subjected to an in-plane shear condition equivalent to that detailed for the 600x1000 mm prototype.

The principal tensile strain and Von Mises stress distributions obtained for the two segments are compared in Figs. 15(a) and 15(b), respectively. In particular, S1 showed a failure mechanism in close agreement with that predicted for the specimen tested, since the two prototypes were characterized by different steel grades but similar layer-to-layer distances. Therefore, collapse mode was proven to be independent on material properties, while the embedment configuration was observed to play a more significant role in the shear response of this solution. When compared to S1, S2 provided a more than doubled (i.e. 2.3) shear capacity and additionally a less ductile behaviour showing larger strain demands concentrated in a significantly smaller portion of the profile; these observations are confirmed by the capacity curves graphed in Fig. 16. Initial stiffness was approximately four times higher than S1 and yielding occurred at an anticipated relative displacement, resulting into a stiffer post-yielding branch, hardened in character. Nonetheless, S1 was roughly 33% more ductile, being the profile freer to deform and plastic strains to distribute in a larger part of it. In addition, a highly non-symmetrical strut-and-tie mechanism was observed to develop and evolve as a consequence of the embedment configuration assumed in the case of S2.

Furthermore, the capacity curves obtained for the three case-studies considered (see Fig. 11-16) were processed to determine the shear force per meter, normalizing the capacity with respect to the total length of the profiles, and finally plotted in Fig. 17 to compare the responses predicted for different steel grades and embedment conditions. Rather than ultimate, the yielding condition may be assumed as a conservative design target and, hence, Table 3 was prepared to collect the yielding shear strengths per meter provided by each solution. Bi-linear approximation, based on a constant-energy idealization, was used for the computations. Assuming the sandwich panel to be attached to the supporting structure through its internal concrete layer only, a comparison is given between the capacity and the demand due to the self-weight of the external RC layer, for various configurations (i.e. number) of intermediate transverse profiles. Even if only two intermediate profiles are used on a 10 m wide panel, the shear demand-to-capacity ratio is still much less than unity. In addition, the maximum bending moment beyond which the steel profiles yield in shear and are no longer able to transfer further coupling forces between the two concrete layers was determined for the considered conditions and summarized in Table 3.

### 3. Behaviour in tension and compression

To predict its tensile and compressive response, the 600x1000 mm subassembly experimentally tested and numerically analyzed in shear was then subjected to a set of uniformly distributed forces out of its plane. Arc-length method was used to solve for the nonlinear equilibrium path. The axial load-end shortening/lengthening capacity curves are provided in Fig. 18, with a top view sketch of the deformed shape under pure tension and compression (i.e. top right and bottom left side). A side view of the failure mechanisms occurred in the stainless steel profile is shown in Fig. 19. Buckling took place under both loading conditions, but the inner curvature at the extremities of the C-shaped profile (see Fig. 2) visibly mitigated its brittleness. If the prototype was loaded in tension, primary strain concentrations locally developed in this junction and, then, the profile opened up before high plastic deformations evolved at mid-stem, in correspondence to the holes, causing it to fail. Further, the positive effect of these notches was evident in compression either, since the collapse mode was characterized by a triple-hinging mechanism. The first two plastic hinges simultaneously formed at

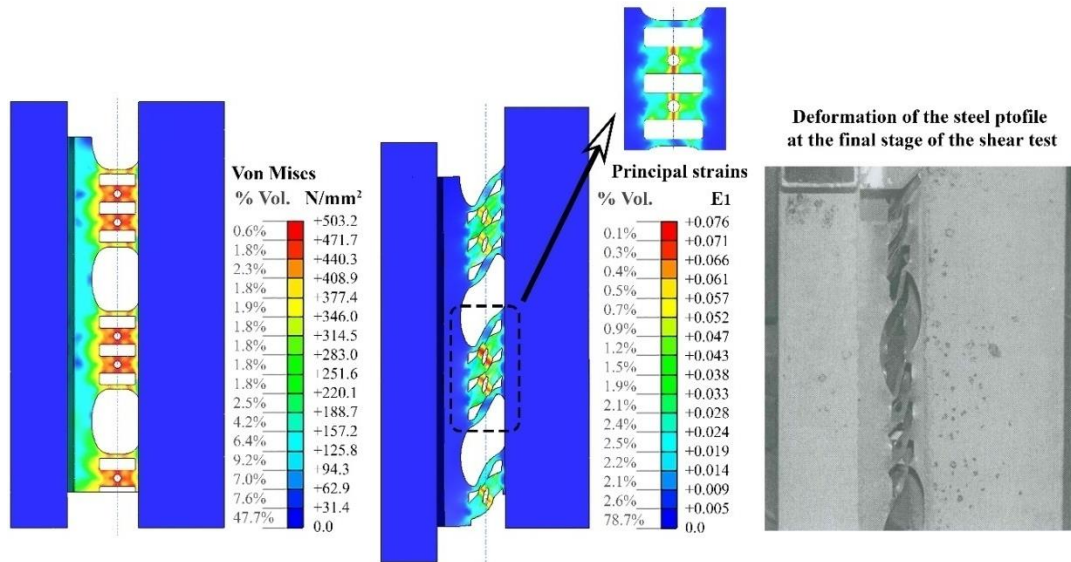


Fig. 12 Experimental vs. numerical failure mechanism: ultimate Von Mises stress and principal tensile strain distribution

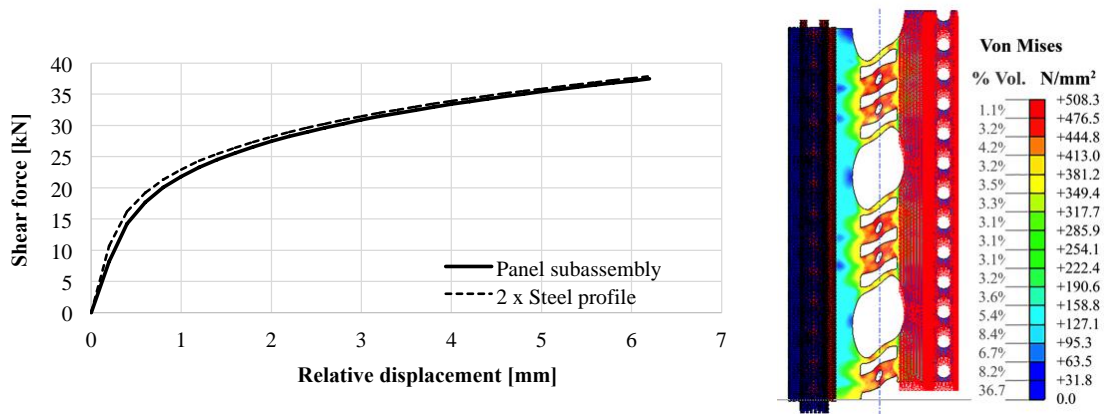


Fig. 13 Shear capacity and steel profile-concrete layer interaction: comparison between FE idealizations

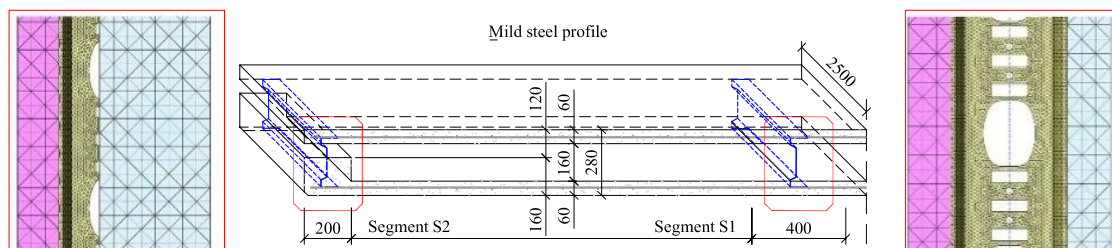


Fig. 14 Schematic of a 10x2.5m panel and geometry of the two reference stripes used for shear analysis



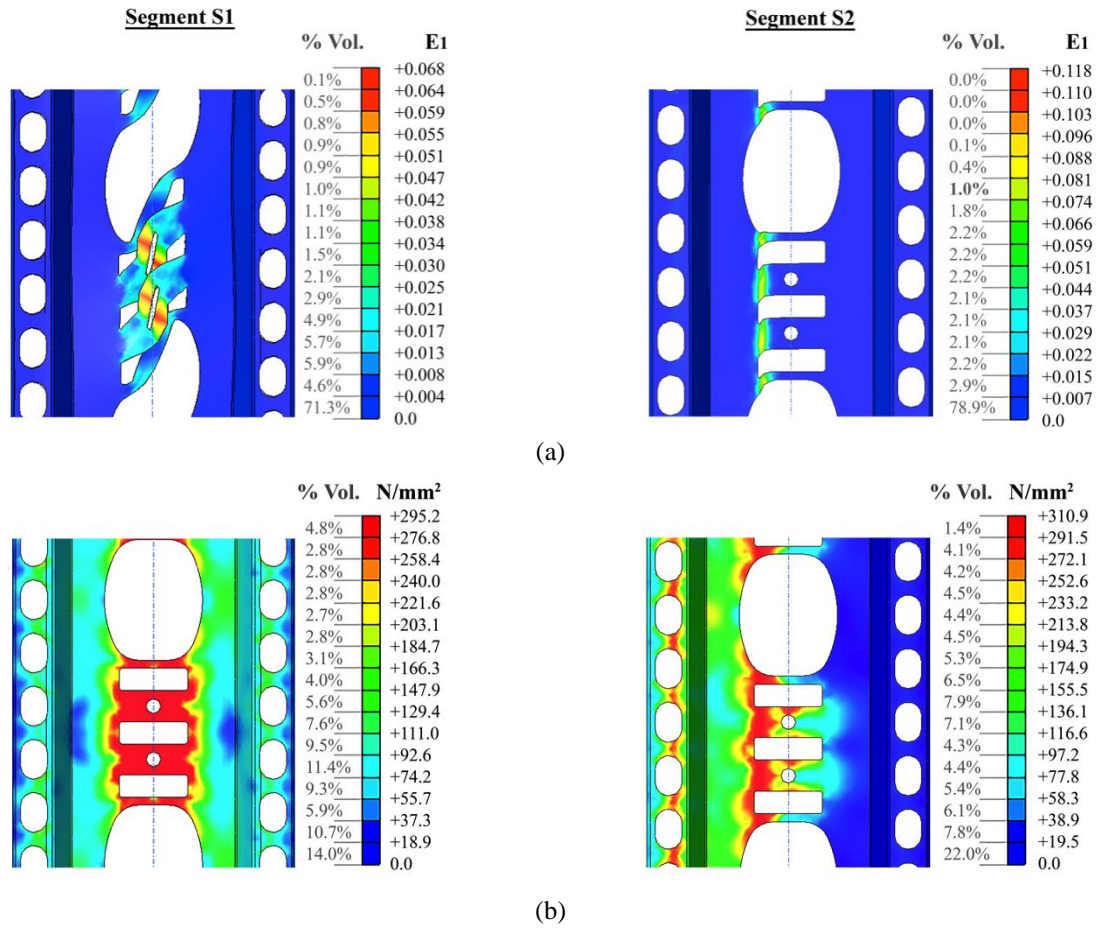


Fig. 15 S1 vs. S2: (a) principal tensile strain and (b) Von Mises stress distributions, at ultimate conditions

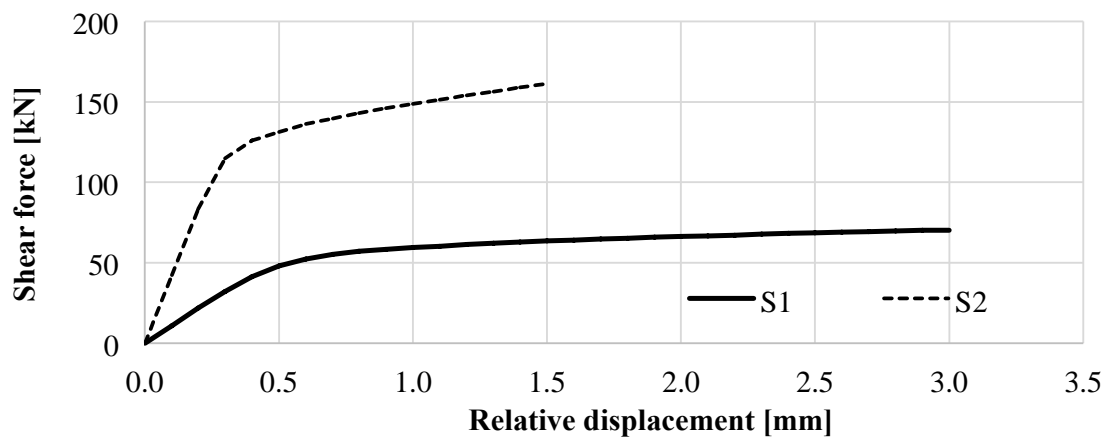


Fig. 16 S1 vs. S2: shear force-relative displacement curves

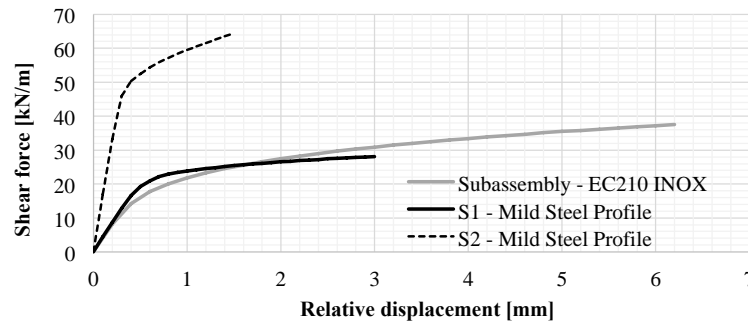


Fig. 17 Shear capacity per length for S1, S2 and subassembly 600x1000 mm

Table 4 Compressive and tensile capacity vs. demand on a steel profile as part of the panel

Configuration			
Compressive and tensile force demand due to self-weight of a concrete layer	3.0÷4.0	3.7÷5.0	4.9÷6.6
Compressive strength (yielding – peak)	66.3 – 72.5		
Tensile strength (yielding – peak)	21.8 – 117.0		

the inner curvatures of the profile, while the third occurred at mid-stem, thus resulting into a weak, but stable softening branch. The comparison between capacity curves revealed yielding to occur in tension at smaller displacement and load levels than compression and, in addition, tensile response was characterized by a much larger global displacement ductility.

As done for shear capacity, both tensile and compressive strength per meter were computed and collected in Table 4, where a comparison is provided with demand values due to self-weight of one RC layer, thus showing such profiles to behave elastically under these loading condition.

#### 4. Construction phases and service conditions

Once assessed the performance of the profile in shear, tension and compression, an entire panel was modelled and analyzed under construction, production and service conditions to reproduce the local stress/strain state of each of its components. The 10x2.5 m sandwich panel, whose S1 and S2 stripes were numerically tested in shear (see Section 2.2.2), was chosen to be representative of this composite technology; the spacing between the mild steel profiles was roughly 2 m. Boundary and loading conditions were prepared to simulate, in an equivalent manner, any stage considered, from formwork to erection on site. Further, concrete properties (i.e. compressive strength) were assumed according to its age at each phase of the construction process. A half or quarter of the panel was, in some cases, studied, given the simple or double symmetry along its axes. The prevailing numerical observations will be summarized in the following.

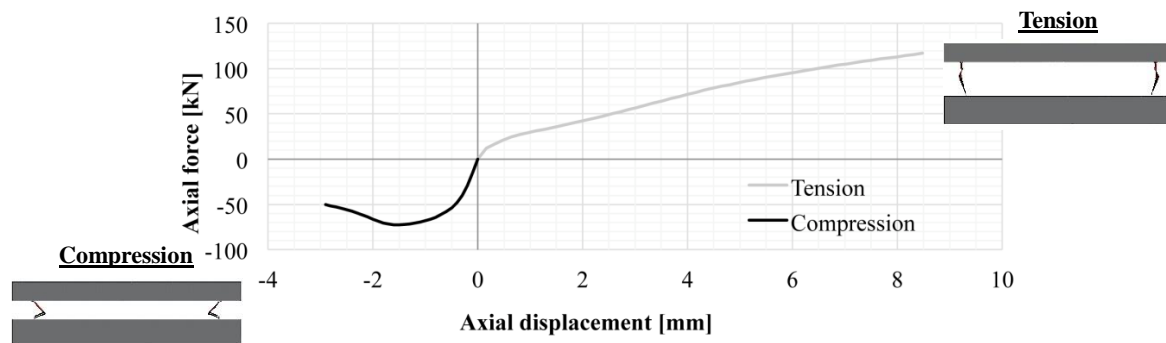


Fig. 18 Specimen 600x1000mm: axial force-displacement curve in tension and compression

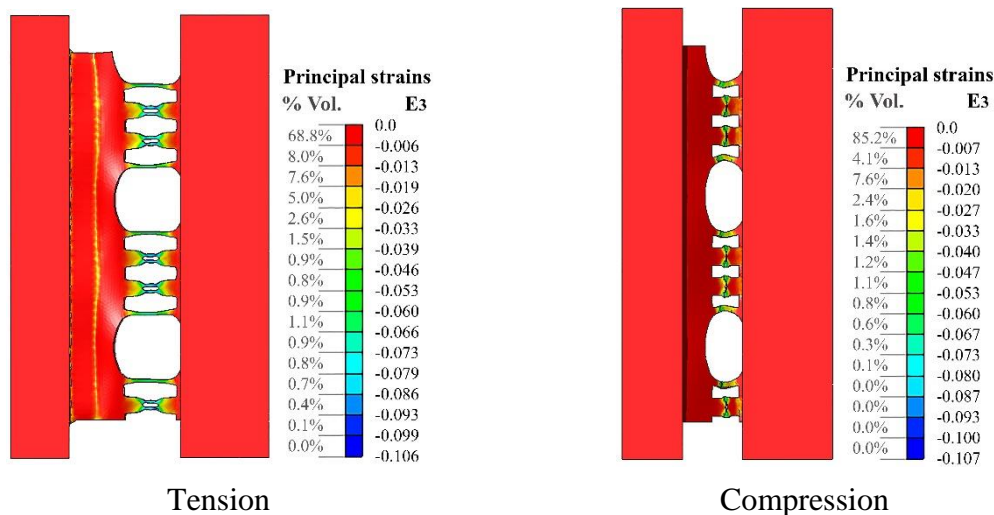


Fig. 19 Failure mechanism under pure tension and compression: principal compressive strains

#### 4.1 Removing from formwork

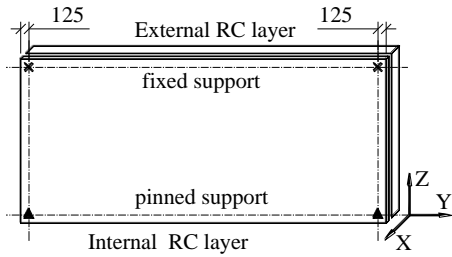
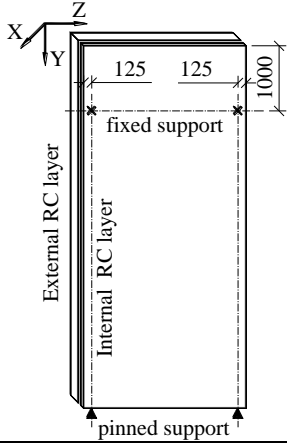
First, the panel was studied while being removed from the formwork; as schematically depicted in Figs. 20(a) and 20(b), two methods of releasing were considered: tilting-up and lifting-up. In detail, the former was played by a set of four overturning forces applied at one long edge, while the latter was managed by eight orthogonal forces used to uplift the panel when still horizontal. Grey arrows are sketched in Figs. 20(a) and 20(b) to schematize these two conditions. In addition, hatched parts are introduced to materialize the segments modelled for each of them. Thus, a half and a quarter of the panel were extracted for tilting-up and lifting-up configurations, accounting for symmetry through a proper set of boundary conditions. Concrete compressive strength was assigned to be 15 MPa, in accordance with its age at this stage. Principal tensile and compressive strains obtained in the most loaded steel profile are collected for both case-studies, thus showing such components to behave in their elastic range. A similar consideration can be drawn for both concrete and mesh reinforcement, which were observed to experience no cracking and yielding, respectively.



#### 4.2 Transport and handling

The stress state of the panel was then investigated during its transport and handling on site. Two different uplift conditions were again analyzed using symmetrical and asymmetrical loading cases, as shown in Fig. 21(a) and 21(b), respectively. The first configuration consisted of a set of four equal forces applied at one long edge with an angle of  $60^\circ$ , while the second was represented by a pair of forces assumed to be 70% and 30% of panel self-weight, in order to simulate its overturning about X-axis. Prior erection on site, concrete compressive strength was selected to be equal to 35 MPa. A half of the panel was analyzed, in the case of symmetrical uplift, while the entire composite system was studied for the second condition, being the loading distribution asymmetrical. As before, none of them made any component work beyond its elastic range. Peaks of the order of  $10^{-4}$  were indeed observed as principal tensile and compressive strains in both steel profile and concrete layer. Mesh reinforcement was again predicted to carry negligibly small stress levels of up to 8 MPa.

Table 5 Service conditions: maximum stress and strain in profile, concrete and reinforcement

			<u>Horizontal panel</u>		<u>Vertical panel</u>	
						
Load	Element					
Self-w	Profile	strains [ $\mu$ ]	$E_1 = 186$	$E_3 = -162$	$E_1 = 1770$	$E_3 = -1570$
		stress [MPa]	$\sigma_{\text{VonMises}} = 28.2$		$\sigma_{\text{VonMises}} = 136.1$	
	Concrete	strains [ $\mu$ ]	$E_1 = 69.8$	$E_3 = 40.7$	$E_1 = 682$	$E_3 = 392$
	Re-bars	stress [MPa]	$\sigma_{\text{max}} = 11.1$	$\sigma_{\text{min}} = -5.9$	$\sigma_{\text{max}} = 5.3$	$\sigma_{\text{min}} = -2.8$
Wind	Profile	strains [ $\mu$ ]	$E_1 = 427$	$E_3 = -386$	$E_1 = 401$	$E_3 = -370$
		stress [MPa]	$\sigma_{\text{VonMises}} = 64.1$		$\sigma_{\text{VonMises}} = 82.6$	
	Concrete	strains [ $\mu$ ]	$E_1 = 106$	$E_3 = 77.2$	$E_1 = 75.0$	$E_3 = 46.3$
	Re-bars	stress [MPa]	$\sigma_{\text{max}} = 17.3$	$\sigma_{\text{min}} = -18.8$	$\sigma_{\text{max}} = 15.8$	$\sigma_{\text{min}} = -14.4$

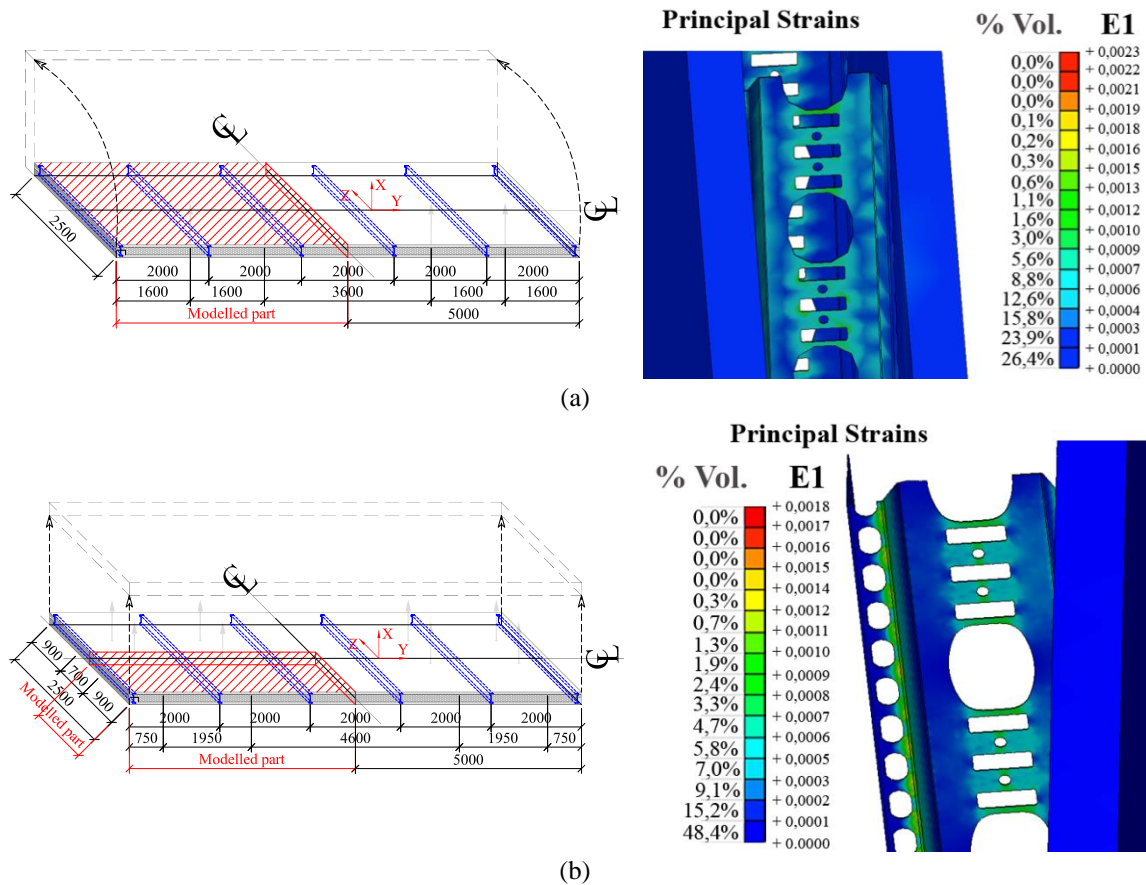


Fig. 20 Removing the panel from the formwork: (a) tilting-up and (b) lifting-up

#### 4.3 Service conditions

The behaviour of this composite system was studied under operational conditions assuming the panel to be horizontally and vertically set in place, according to the two configurations sketched in Table 5. When horizontal, its top two corners were assumed to be fixed to the supporting structure, while the bottom two were simply supported. Similar boundary conditions were applied in the case of vertical panels, but the top two supports were placed at a 1 m inward distance from the short top edge of the panel. Self-weight and wind were considered for both configurations. In detail, a value of 0.7 kN/m<sup>2</sup> was uniformly distributed to load the external layer of the prototype out-of-plane. As done for transport and handling, concrete compressive resistance was assigned to be 35 MPa in the simulations. Table 5 was prepared to summarily describe the stress/strain state of the two sandwich panels and their components, confirming them to behave elastically even under service conditions.

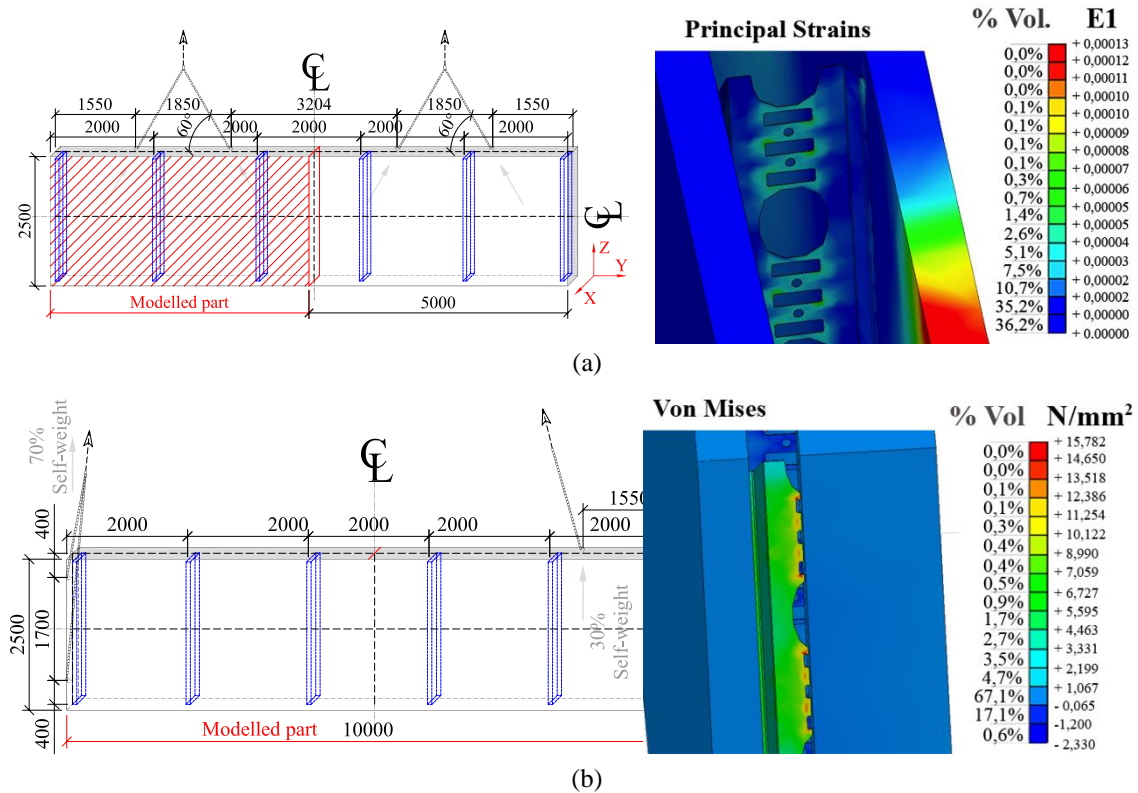


Fig. 21 Transport and handling by (a) symmetrical and (b) asymmetrical force configuration

## 5. Conclusions

The numerical study described herein was conducted to investigate the large displacement-large strain inelastic response of a cold-drawn steel profile for multi-layered sandwich panels. Modeling procedures for characterizing its behaviour under shear, tension and compression were prepared, in compliance with experimental observations. High-definition FE idealizations, based on traditional nonlinear fracture mechanics and yielding criterion, were developed, including in the analysis steel profile-concrete layers interaction, in a phenomenological sense, via bond-slip constitutive laws. In addition, the structural performance of this composite technology was assessed at each stage of the production process, from formwork to service conditions. The prevailing conclusions, drawn from this research, can be summarized as follows

- Numerical estimates obtained for preliminary pull and pull-out tests on a stainless steel tie revealed a satisfying and safe match with experimental observations, thus validating the calibration of the constitutive laws assumed for steel and concrete members, as well as for their interaction.
- The modeling approach implemented was shown to be effective when applied for shear strength assessment of such systems. Von Mises stress and principal strain distributions

in close agreement with the experimental failure mode were predicted. The high plastic strain concentrations observed in the profiles, as a consequence of the strut-and-tie path, did not cause any anticipated net fracture, whilst a gradual evolution of its deformation pattern was evidenced, in tests and FE simulations. Concrete was proven to experience no damage except minor cracking in small volumes adjacent to the profile, where stress levels slightly less than peak tensile strength were still able to be transmitted across the cracks. Hence, profile-concrete connection can be acceptably considered to be fixed.

- Sensitivity of shear response to steel type and concrete layer-to-layer gap was assessed, in terms of failure mechanism and shear force-displacement curves. The collapse mode was found to be independent on steel characteristics, whilst a more significant role was played by the embedment configuration, which was observed to visibly affect stiffness, strength and ductility of the subassembly.
- Buckling occurred both in tension and compression, but the inner curvature at the ends of the C-shaped profile mitigated the mechanism. In tension, local strain concentrations developed in these junctions and the profile opened up before high plastic deformations evolved at mid-stem, causing it to collapse. Due to these notches, a triple-hinging mode took place, with two hinges simultaneously formed at the inner curvatures of the profile and a third occurred at mid-stem, thus resulting into a weak, but stable softening branch. Yielding occurred in tension at smaller displacement and force levels than compression and, in addition, a much more ductile response was determined.
- Under construction phases and service conditions, the series of detailed FE simulations showed the panel to behave elastically. The stress/strain state of each of its components confirmed yielding not to take place in steel profiles and mesh reinforcement. Similarly, no cracking was observed to occur in concrete layers for any loading phase considered. Up to this load level, the steel profile was demonstrated to be able to effectively couple the two RC layers, without exhibiting any permanent plastic deformation.

## Acknowledgments

The authors would like to express their gratitude to B.S. Italia – Gruppo Styl-Comp for having financed the numerical research described in this paper, through a one year framework programme established with the European Centre for Training and Research in Earthquake Engineering.

## References

- Adalier, K. and Aydingun, O. (2001), “Structural engineering aspects of the June 27, 1998 Adana-Ceyhan (Turkey) earthquake”, *Eng. Struct.*, **23**(4), 343-355.
- Architectural Precast Concrete (2007), Chicago, Illinois: PCI Architectural Precast Concrete Manual Committee. (Vols. 3rd Edition, First Printing).
- Belleri, A., Brunesi, E., Nascimbene, R., Pagani, M. and Riva, P. (2014), “Seismic performance of precast industrial facilities following major earthquakes in the Italian territory”, *J. Perform. Constr. Fac. -ASCE*, DOI: 10.1061/(ASCE)CF.1943-5509.0000617.
- Biscaia, H.C., Chastre, C. and Silva, M.A.G. (2013), “A smeared crack analysis of reinforced concrete T-beams strengthened with GFRP composites”, *Eng. Struct.*, **56**, 1346-1361.
- Bournas, D.A., Negro, P. and Taucer, F.F. (2014), “Performance of industrial buildings during the Emilia

- earthquakes in Northern Italy and recommendations for their strengthening”, *Bull. Earthq. Eng.*, **12**(5), 2383-2404.
- Brunesi, E., Nascimbene, R., Bolognini, D. and Bellotti, D. (2015a), “Experimental investigation of the cyclic response of reinforced precast concrete framed structures”, *PCI J.*, **60**(2), 57-79.
- Brunesi, E., Bolognini, D. and Nascimbene, R. (2015b), “Evaluation of the shear capacity of precast-prestressed hollow core slabs: numerical and experimental comparisons”, *Mater. Struct.*, **48**(5), 1503-1521. DOI: 10.1617/s11527-014-0250-6.
- Brunesi, E., Nascimbene, R., Pagani, M. and Beilic, D. (2014a), “Seismic performance of storage steel tanks during the May 2012 Emilia, Italy, earthquakes”, *J. Perform. Constr. Fac. -ASCE*, DOI: 10.1061/(ASCE)CF.1943-5509.0000628.
- Brunesi, E., Nascimbene, R. and Rassati, G.A. (2014b), “Response of partially-restrained bolted beam-to-column connections under cyclic loads”, *J. Constr. Steel. Res.*, **97**, 24-38.
- Brunesi, E., Nascimbene, R. and Rassati, G.A. (2015c), “Seismic response of MRFs with partially-restrained bolted beam-to-column connections through FE analyses”, *J. Constr. Steel. Res.*, **107**, 37-49.
- Brunesi, E. and Nascimbene, R. (2014), “Extreme response of reinforced concrete buildings through fiber force-based finite element analysis”, *Eng. Struct.*, **69**, 206-215.
- Casarotti, C. and Pinho, R. (2006), “Seismic response of continuous span bridges through fiber-based finite element analysis”, *Earthq. Eng. Vib.*, **5**(1), 119-131.
- Charney, F.A. and Harris, J.R. (1989), *The Effect of Architectural Precast Concrete Cladding on the Lateral Response of Multistory Buildings*, Chicago, Illinois: PCI.
- Dörr, K. (1980), *Ein Beitrag zur Berechnung von Stahlbetonscheiben unter besondere Berücksichtigung des Verbundverhaltens*. PhD Thesis, University of Darmstadt.
- Ghosh, S.K. and Cleland, N. (2012), “Observations from the February 27, 2010, earthquake in Chile”, *PCI J.*, **57**(1), 52-75.
- Girão Coelho A.M. (2013), “Rotation capacity of partial strength steel joints with three-dimensional finite element approach”, *Comput. Struct.*, **116**, 88-97.
- Henry, R.M. and Roll, F. (1986), “Cladding-Frame Interaction”, *J. Struct. Eng. - ASCE.*, **112**(4), 815-834.
- Hordijk D.A. (1991), *Local Approach to Fatigue of Concrete*. PhD thesis, Delft University of Technology.
- Hung, C.C. and El-Tawil, S. (2010), “Hybrid rotating/fixed-crack model for high performance fiber reinforced cementitious composites”, *ACI Mater. J.*, **107**(6), 569-577.
- Hung, C.C. and Li, S.H. (2013), “Three-dimensional model for analysis of high performance fiber reinforced cement-based composites”, *Compos. B. Eng.*, **45**(1), 1441-1447.
- Hung, C.C., Su, Y.F. and Yu, K.H. (2013), “Modeling the shear hysteretic response for high performance fiber reinforced cementitious composites”, *Constr. Build. Mater.*, **41**, 37-48.
- Hunt, J.P. and Stojadinovic, B. (2010), *Seismic Performance Assessment and Probabilistic Repair Cost Analysis of Precast Concrete Cladding Systems for Multistory Buildings*. PEER.
- Le Nguyen, K., Brun, M., Limam, A., Ferrier, E. and Michel, L. (2014), “Pushover experiment and numerical analyses on CFRP-retrofit concrete shear walls with different aspect ratios”, *Compos. Struct.*, **113**, 403-418.
- Liberatore, L., Sorrentino, L., Liberatore, D. and Decanini, L.D. (2013), “Failure of industrial structures induced by the Emilia (Italy) 2012 earthquakes”, *Eng. Fail. Anal.*, **34**, 629-647.
- Magliulo, G., Ercolino, M., Petrone, C., Coppola, O. and Manfredi, G. (2014), “Emilia Earthquake: the Seismic Performance of Precast RC Buildings”, *Earthq. Spectra.*, **30**(2), 891-912.
- Medina, R.A., Sankaranarayanan, R. and Kingston, K.M. (2006), “Floor response spectra for light components mounted on regular moment-resisting frame structures”, *Eng. Struct.*, **28**(14), 1927-1940.
- MIDAS (2010) Nonlinear and Detail FE Analysis System for Civil Structures - FEA Analysis and Algorithm Manual (www.cspfea.net).
- Mosqueda, G., Retamales, R., Filiatrault, A. and Reinhorn, A. (2009), “Testing facility for experimental evaluation of non-structural components under full-scale floor motions”, *Struct. Des. Tall. Spec.*, **18**(4), 387-404.
- Mpampatsikos, V., Nascimbene, R. and Petrini, L. (2008), “A critical review of the R.C. frame existing

- building assessment procedure according to Eurocode 8 and Italian Seismic Code”, *J. Earthq. Eng.*, **12**(1), 52-82.
- Pecce, M., Ceroni, F., Bibbò, F.A. and De Angelis, A. (2014), “Behaviour of RC buildings with large lightly reinforced walls along the perimeter”, *Eng. Struct.*, **73**, 39-53.
- Petrone, C., Magliulo, G. and Manfredi, G. (2014), “Shake table tests for the seismic assessment of hollow brick internal partitions”, *Eng. Struct.*, **72**, 203-214.
- Retamales, R., Mosqueda, G., Filiatrault, A. and Reinhorn, A. (2011), “Testing protocol for experimental seismic qualification of distributed nonstructural systems”, *Earthq. Spectra.*, **27**(3), 835-856.
- Retamales, R., Davies, R., Mosqueda, G. and Filiatrault, A. (2013), “Experimental seismic fragility of cold-formed steel framed gypsum partition walls”, *J. Struct. Eng. - ASCE*, **139**(2), 1285-1293.
- Sezen, H. and Whittaker, A.S. (2006), “Seismic performance of industrial facilities affected by the 1999 Turkey earthquake”, *J. Perform. Constr. Fac. -ASCE*, **20**(1), 28-36.
- Spacone, E., Filippou, F.C. and Taucer, F.F. (1996), “Fibre beam-column model for non-linear analysis of RC frames: part I. Formulation”, *Earthq. Eng. Struct. D.*, **25**, 711-725.
- Taghavi, S. and Miranda, E. (2003), *Response Assessment of Nonstructural Building Elements*. University of California. Berkeley: PEER.
- Thorenfeldt, E., Tomaszewicz, A. and Jensen, J.J. (1987), “Mechanical properties of high-strength concrete and applications in design”, In: *Proceedings symposium utilization of high-strength concrete*, Trondheim, Norway, Tapir.
- Toniolo, G. and Colombo, A. (2012), “Precast concrete structures: the lessons learned from the L’Aquila earthquake”, *Struct. Concr.*, **13**(2), 73-83.
- Vecchio, F.J. and Collins, M.P. (1986), “The modified compression field theory for reinforced concrete elements subjected to shear”, *ACI Struct. J.*, **83**(2), 219-231.
- Vecchio, F.J. and Collins, M.P. (1993), “Compression response of cracked reinforced concrete”, *J. Struct. Eng. -ASCE*, **119**(12), 3590-3610.
- Venini, P. and Nascimbene, R. (2003), “A new fixed-point algorithm for hardening plasticity based on non-linear mixed variational inequalities”, *Int. J. Numer. Meth. Eng.*, **57**(1), 83-102.
- Villaverde, R. (2006), “Simple method to estimate the seismic nonlinear response of nonstructural components in buildings”, *Eng. Struct.*, **28**(8), 1209-1221.
- Wanitkorkul, A. and Filiatrault, A. (2008), “Influence of passive supplemental damping systems on structural and nonstructural seismic fragilities of a steel building”, *Eng. Struct.*, **30**(3), 675-682.